ACS OMEGA

http://pubs.acs.org/journal/acsodf

Article

Physical and Biological Properties of 5-Fluorouracil Polymer-Coated Magnetite Nanographene Oxide as a New Thermosensitizer for Alternative Magnetic Hyperthermia and a Magnetic Resonance Imaging Contrast Agent: In Vitro and In Vivo Study

Leila Kiamohammadi, Leili Asadi, Sakine Shirvalilou, Samideh Khoei,* Sepideh Khoee, Maryam Soleymani, and Soraya Emamgholizadeh Minaei

Cite This: *ACS Omega* 2021, 6, 20192−20204

Read Online

ACCESS | Metrics & More | Article Recommendations

ABSTRACT: This study reports a new procedure for utilizing 5-fluorouracil (5-Fu)-loaded polycaprolactone (PCL)/chitosan-covered magnetite nanographene oxide (5-Fu/SPION/NGO@PCL−LMWC) as a platform for synergistic thermo−chemotherapy. In fact, superparamagnetic iron oxide nanoparticles/nanographene oxide (SPION/NGO) nanoparticles can be coated with copolymers PCL/chitosan to attain better colloidal stability in the biological environment. Nanoparticles were synthesized and characterized for their size, surface charge, X-ray patterns, polymer content, and in vitro heat-triggered release. In vitro cytotoxic effects of nanoparticles on CT-26 cells were assessed with an MTT assay and real-time polymerase chain reaction. In vivo tumor growth inhibition was evaluated on an allograft mouse model of CT-26 cells. Tumor-bearing mice were injected with 5-Fu-loaded nanoparticles intravenously, and then, the targeted delivery was amplified using a magnetic field and finally exposed to an alternating magnetic field (AMF) (40 A/m, 13.56 MHz), during which the tumor site temperature increased to 43 °C. By using an infrared camera, we managed to heat the nanoparticles up to a constant temperature between 42.5 and 43.5 °C, with a tolerance ±0.03 °C. Finally, in vitro results showed that 5-Fu-loaded nanoparticles combined with AMF hyperthermia significantly reduced the plating efficiency of the cells ($P < 0.01$) and increased the Bax/Bcl-2 ratio (1.42 times, $P < 0.01$) compared with those achieved with each one alone. Furthermore, in vivo results demonstrated that the treatment of 5-Fu-loaded nanoparticles combined with the AMF diminished the growth of CT-26 tumor cells and increased the life span of the tumor-bearing mice ($P < 0.001$) by thermal energy deposition compared to that of the free 5-Fu drug. Also, the high level of accumulation of the nanoparticles within the tumor site was easily monitored with magnetic resonance imaging. It was concluded that the multifunctional magnetic nanoparticles could be used as a promising nanocarrier platform for achieving concurrent goals, drug delivery, magnetic targeting, thermal-sensitizing, cell death induction, and real-time monitoring of response to treatment.

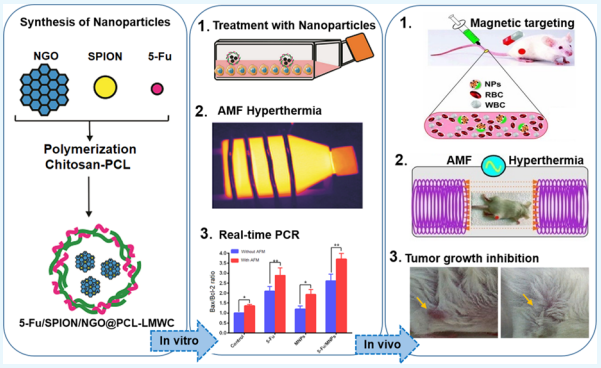

1. INTRODUCTION

Hyperthermia (HT), known as green therapy, is widely applied as an adjuvant therapy with chemo and/or radiotherapy in the treatment of patients with malignant tumors, resulting in significant enhancement of the cancer therapy outcome.[1] Among various heating procedures, magnetic induction HT based on iron oxide nanoparticles (MH) has potential to achieve an optimal therapeutic efficiency due to its ability to transfer enough heating power to deep-seated tissues and mediate a controlled release of the therapeutic agents.[2,3] The principle of MH is to use magnetic nanoparticles (MNPs) under an alternating magnetic field (AMF) to absorb and convert the electromagnetic energy into heat (41−45 °C) through magnetic moment rotation (Néel relaxation) and/or physical rotation (Brown relaxation).[4] Since the tumor cells are more sensitive to rapid increases in temperature than the normal neighbor cells, this temperature enhancement can induce death of the tumor cells.[5,6]

For this purpose, superparamagnetic nanoparticles (SPIONs) have drawn the attention of researchers as efficient cancer HT materials, drug-targeting carriers via applying an

Received: April 1, 2021
Accepted: July 15, 2021
Published: July 28, 2021

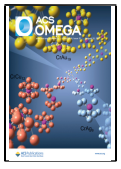

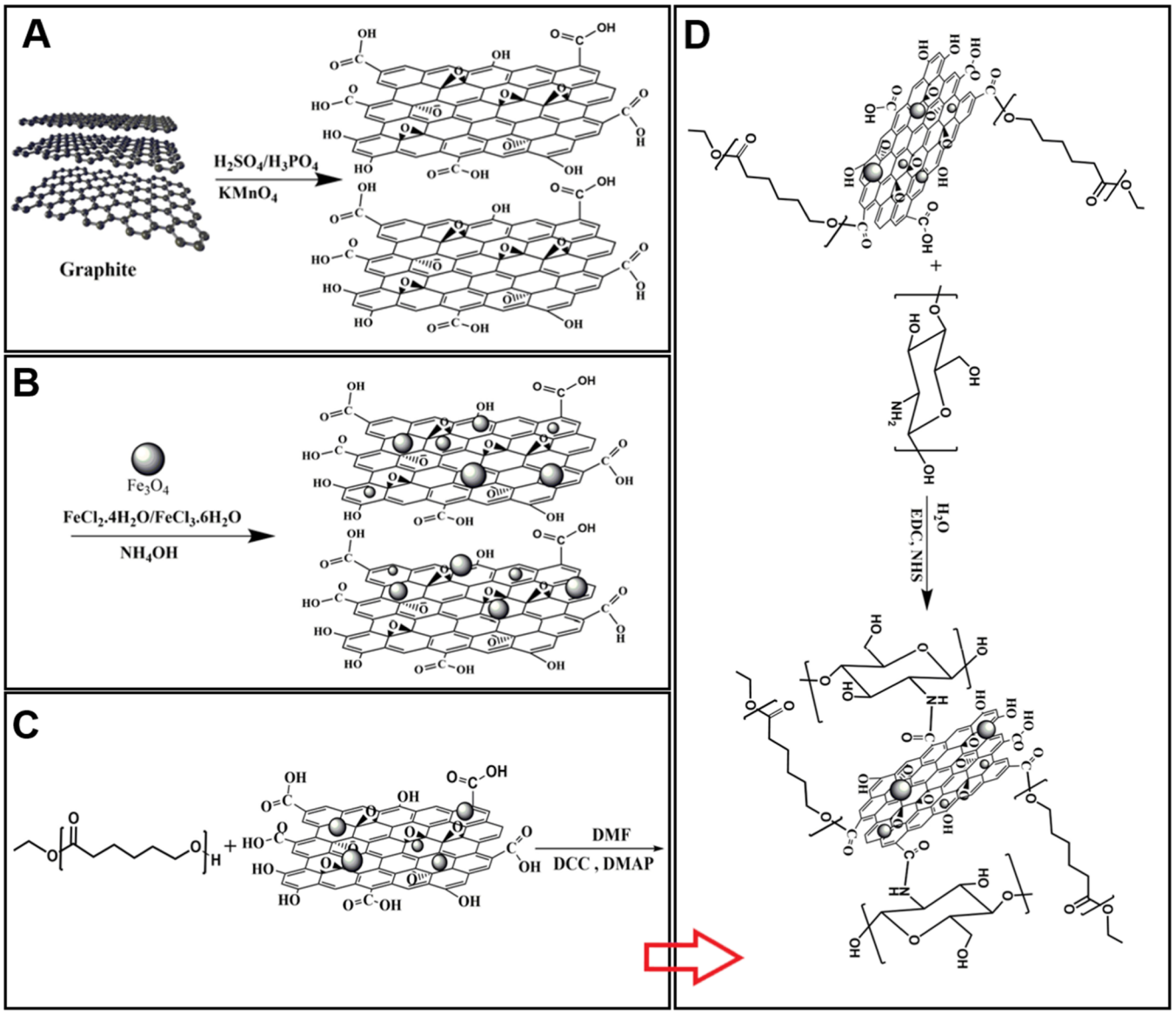

Figure 1. A) Synthesis of GO, (B) SPION/NGO, (C) SPION/NGO@PCL, and (D) SPION/NGO@PCL−LMWC nanoparticles.

external magnetic field at tumor sites,[7] and magnetic resonance imaging (MRI) contrast agents.[8] However, on the other hand, SPIONs have a weak magnetic response due to low magnetism.[9] To compensate for this problem, a high concentration of SPIONs, high-intensity magnetic fields, or a high frequency must be used.[10] However, there is always a practical limit to the maximum application of these parameters. The frequency and magnetic field range should fall within the clinically accepted AMF limits ($H_f < 5 \times 10^9$ A/ms).[11,12]

Clinical studies have illustrated that HT, when combined with chemotherapy, drastically raises the cytotoxicity of chemotherapeutic agents.[5,13] The interaction among heat and anticancer agents increases the drug accumulation at the tumor site by increasing the local blood flow and endothelial cell permeability.[14] In these situations, multiple side effects of the anticancer drugs could be diminished by a suitable decline of the drug dose.[15] Multiple studies showed that the entrapment of anticancer agents in polymer-coated SPIONs optimizes their therapeutic efficiency and decreases side effects, in contrast to conventional anti-cancer drugs.[16] Nanographene oxide (NGO) has also become popular for its high drug-loading efficiency, excellent colloidal stability, and high biocompatibility.[17] Sugumaran et al. demonstrated that coating nanoparticles with NGO sheets significantly improved their colloidal stability.[9]

In a previous work, we observed the effects of magnetite NGO-based nanocarrier on the cell death mechanisms following MH treatment.[18] Other studies have described the mechanisms of cell death caused by magnetic HT. However, in all these studies, the evaluation of the effect of MH therapy on the molecular mechanisms determining different pathways of apoptosis has not been given much attention.[19]

In the present study, we investigated alterations in the cell death mechanisms of the CT-26 mouse colon cancer cell line associated with chemo-thermotherapy and the thermal behavior of colon-tumor-bearing BALB/c mice when exposed to an AMF (13.56 MHz) in the presence of SPION−NGO@PCL−LMWC (MNPs) containing 5-fluorouracil (5-Fu). The 5-Fu-loaded MNPs were selectively accumulated in the solid tumor of tumoral BALB/c mice under external magnetic fields (0.22 T) with a high efficiency, allowing the location of the colorectal tumors to be delineated by MRI. However, despite

https://doi.org/10.1021/acsomega.1c01763
ACS Omega 2021, 6, 20192−20204

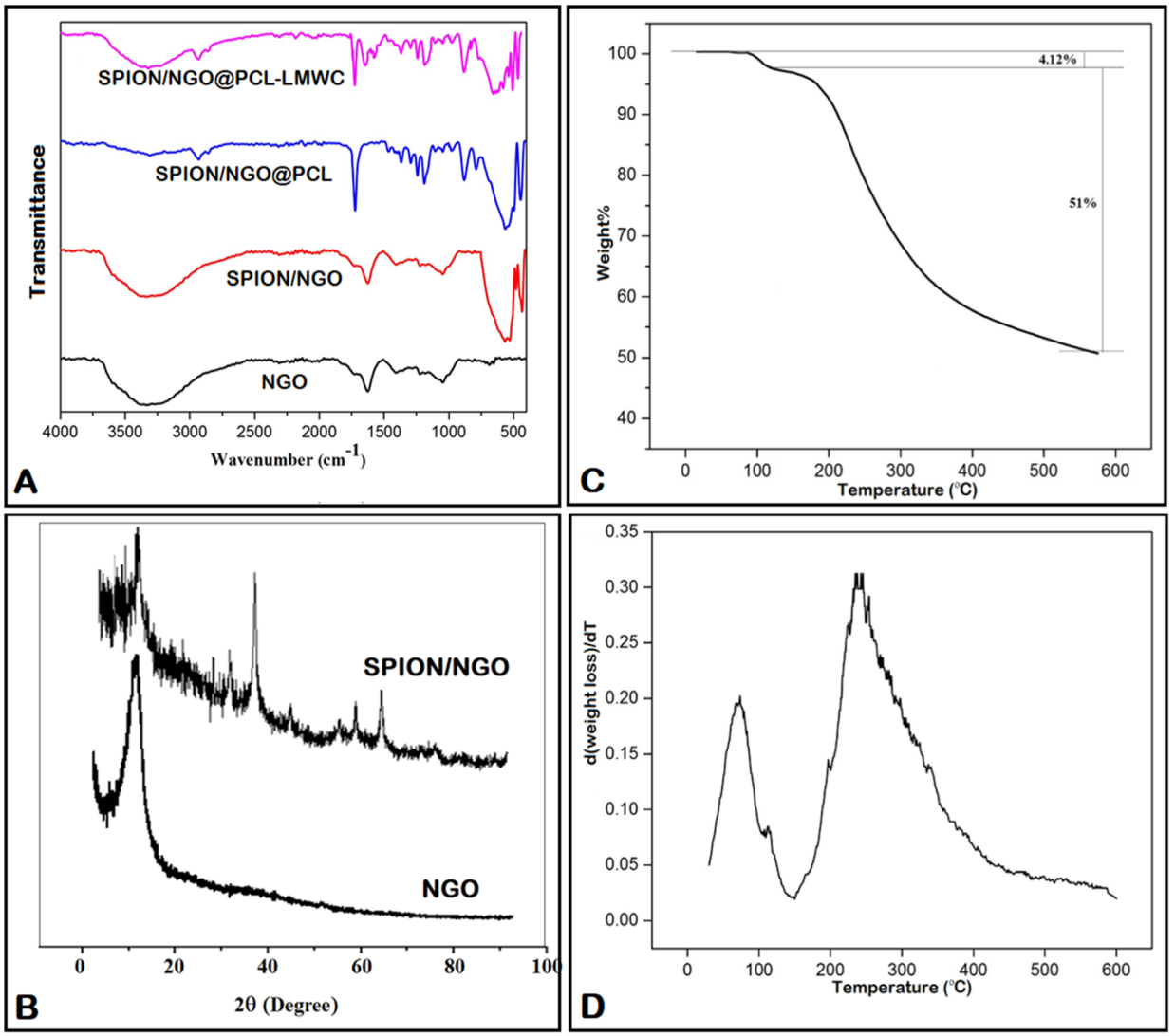

Figure 2. A) FT-IR spectra of SPION/NGO@PCL−LMWC nanoparticles, (B) XRD patterns of NGO and SPION/NGO, and (C) TGA and (D) DTG curves of SPION/NGO@PCL−LMWC nanoparticles.

the great potential of MNPs for the magnetic targeting procedure, there is still a major challenge to achieving a uniform drug distribution in the total volume of solid tumors. Furthermore, prolonged survival time, weight changes, and therapeutic efficacy were evaluated in mice with CT-26 malignant colon tumors.

2. RESULTS

2.1. Characterization of Nanoparticles. GO nanosheets were prepared through the improved Hummer's method by the oxidation of graphite flakes (Figure 1A). Fourier-transform infrared spectroscopy (FT-IR) results referring to NGO showed a broad adsorption at 3300−3500 cm^{-1}, which was attributed to the stretching vibration frequency of −OH groups. Additionally, the observed peaks at 1725 and 1626 cm^{-1} were attributed to C═O and C═C bonds of the carboxylic and aromatic hydrocarbon groups, respectively (Figure 2A). The X-ray diffraction (XRD) pattern of NGO in Figure 2B shows a distinct peak at 2θ = 10.28°, which was related to GO sheets. Comparison of the FT-IR spectra of SPION/NGO (Figure 2A) and NGO showed a sharp peak at 588 cm^{-1}, which can be attributed to the Fe−O stretching vibration, indicating a modification of the NGO surface with iron oxide nanoparticles. SPION/NGO formation was also confirmed by XRD analysis, in which the new peaks detected at 2θ of 30.3, 35.67, 43.25, 53.7, 57.43, and 62.6° were attributed to the crystalline structure of iron oxide nanoparticles (Figure 2B). The prepared SPION/NGO nanoparticles were functionalized with polycaprolactone (PCL) (Figure 1C) and low-molecular-weight chitosan (LMWC) (Figure 1D) under esterification and amidation reaction conditions, respectively. The FT-IR spectrum of SPION/NGO@PCL nanoparticles is illustrated in Figure 2A. As shown, the characteristic peaks observed at 1725 and 2880 cm^{-1} are due to the stretching vibration of C═O and $-CH_2$ groups of PCL, respectively, confirming the successful modification of SPION/NGO with PCL. Furthermore, the FT-IR spectrum of the SPION/NGO@PCL−LMWC nanoparticles is shown in Figure 2A. The appearance of two peaks at 1650 and 1574 cm^{-1} was due to the carbonyl stretching bond and N−H bending of amide groups of LMWC, respectively.

Thermal analysis was used to evaluate the polymer content of SPION/NGO@PCL−LMWC nanoparticles. As shown in

https://doi.org/10.1021/acsomega.1c01763
ACS Omega 2021, 6, 20192−20204

Table 1. Particles Size and Zeta Potential of the Nanoparticles (n = 3)

type of nanoparticles	particle size (nm)	PDI	zeta potential
SPION/NGO@PCL−LMWC	43.4 ± 1.9	0.182	−30.22 ± 0.21
5-Fu/SPION/NGO@PCL−LMWC	79.1 ± 3.9	0.265	−13.39 ± 0.46

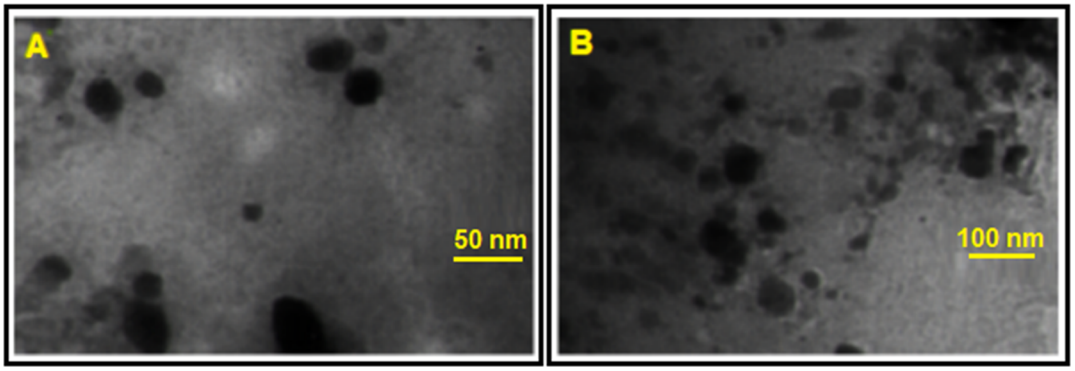

Figure 3. TEM images of (A) SPION/NGO@PCL−LMWC and (B) 5-Fu-loaded SPION/NGO@PCL−LMWC.

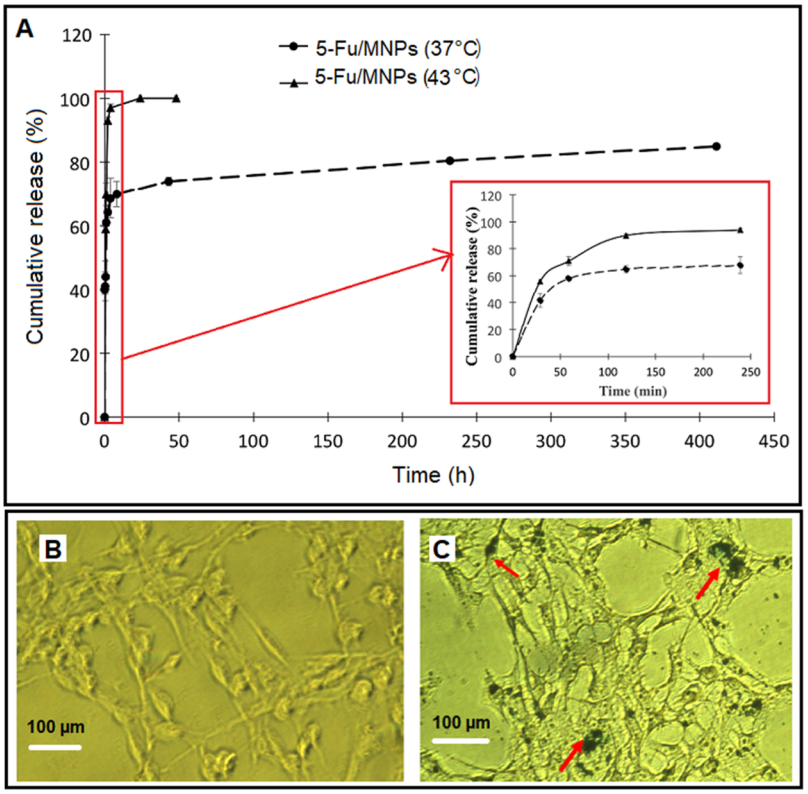

Figure 4. A) In vitro release profiles of 5-Fu from 5-Fu/SPION/NGO@PCL−LMWC at 37 and 43 °C (n = 3). Detection of intracellular iron oxide nanoparticles using Prussian blue staining: (B) control and (C) 5-Fu/SPION/NGO@PCL−LMWC. Arrows indicate iron oxide nanoparticles.

Figure 2C, the weight loss of 4.12% observed at 100 °C could be attributed to the evaporation of water absorbed in the sample. Due to the decomposition of grafted polymers, the nanoparticles lost 51% of their weight from 230 to 600 °C, indicating the conjugation of polymers on SPION/NGO. The derivative of thermogravimetry analysis (TGA) curve (DTG) showed two main decomposition temperatures at around 80 and 250 °C due to the loss of water molecules and degradation of both polymers with the initial and final temperatures of approximately 150 °C and completion by 550 °C, respectively (Figure 2D).

The particle size and zeta potential of nanoparticles are strongly influenced by the emulsifier used in the production process. The results of the particle size, polydispersity index (PDI), and zeta potential of both types of MNPs are presented in Table 1. The average size of all nanoparticles showed a mean diameter of below 100 nm in the phosphate-buffered saline (PBS) solution. After loading 5-Fu into MNPs, the size of the MNPs increased obviously from about 44 nm to about 80 nm.

https://doi.org/10.1021/acsomega.1c01763
ACS Omega 2021, 6, 20192−20204

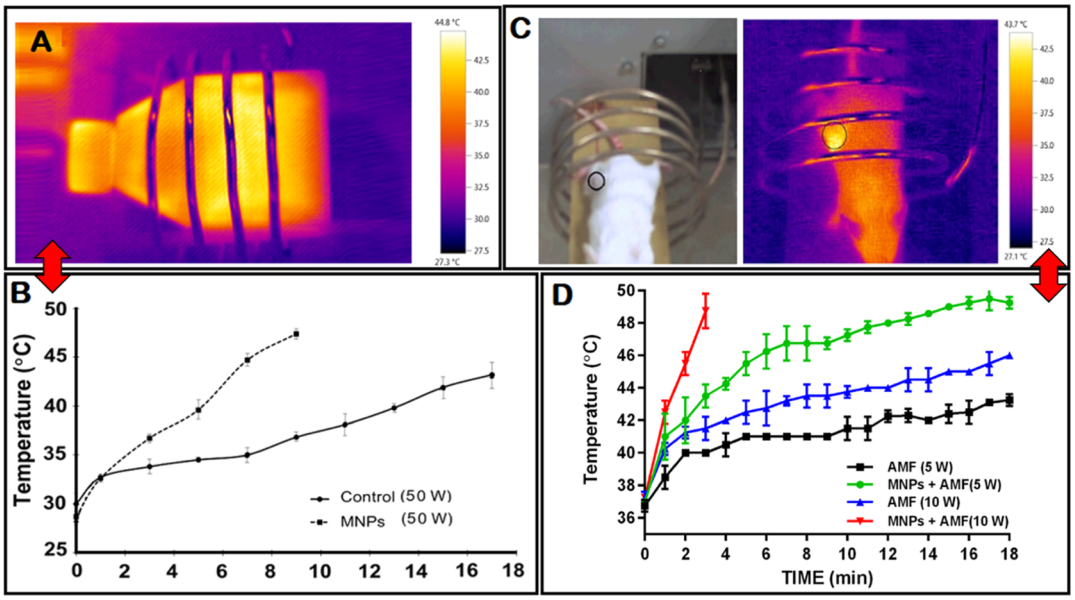

Figure 5. A) Thermal distribution profile of the cells under an AMF and (B) increasing temperature profiles of the CT-26 cells treated with SPION/NGO@PCL−LMWC nanoparticles and control (without MNPs) groups under an AMF as a function of time. (C) Mean temperature curve during heating measured by an IR camera for mice positions in the AMF coil. Black dashed circle shows the location of the colorectal tumor. (D) Temperature−time curve with 13.56 MHz alternating RF magnetic field at powers of 5 and 10 W.

Zeta potentials of MNPs and 5-Fu loaded MNPs were −30 and −13 mV, respectively. This decrease in the zeta potential was attributed to the anionic nature of 5-Fu. Transmission electron microscopy (TEM) analysis was used to describe the morphology of nanoparticles, which showed that most of the nanoparticles had a spherical shape, and the average particle size was less than 100 nm (Figure 3A,B). Furthermore, the drug content and encapsulation efficiency of the PCL−LMWC-coated nanoparticles were 2.9 and 92%, respectively.

2.2. In Vitro Release Profile of 5-Fu. According to the results, the release of 5-Fu in the first 24 h was 68.965 ± 1.48% at 37 °C (Figure 4A). The total release from MNPs at 37 °C over 7 days was 81%. Additionally, a rapid release of 5-Fu was observed in the first hour for MNPs at 43 °C. The 5-Fu release within 4 h was equivalent to 97% release for PCL−LMWC-coated MNPs at 43 °C. Clearly, the heat increased the release of 5-Fu from MNPs.

2.3. In Vitro Experiments. *2.3.1. Prussian Blue Staining.* Figure 4B,C shows the control cells without MNP treatment and also indicate the internalization of nanoparticles containing 11.8 μg/mL of iron oxide into CT-26 cells. Blue spots represent MNPs. Also, at this concentration (0.1 mg of MNPs), the cell viability was above 95% (as shown in Figure 6). Due to the low concentration and low toxicity at this concentration, the cells were not damaged and the cell structure, especially the cell membrane, was not affected.

2.4. AMF Irradiation and Thermometry: In Vitro and In Vivo. In vitro: to evaluate the prerequisite duration of HT at 43 °C, flasks treated with nanoparticles were irradiated with AMF and monitored with an IR camera. Figure 5A,B shows the increasing temperature profiles of the cells as a function of time. The mean temperature of the cells irradiated with an AMF increased to 43° C in 17 min for the control and in 43 min for the SPION/NGO@PCLLMWC group.

In vivo: mean temperature curves for the mice colorectal tumor area, as measured by the IR camera, are shown in Figure 5C,D. These results indicated that temperature changes depend on the alternating radiofrequency (RF) magnetic field power and the presence of MNPs. Figure 5D shows how the temperature of the tumor exposed to the AMF (13.56 MHz, 5 W) slowly increased over a period of 18 min to reach 43 °C. This was reported to be less than about 8 min for a power of 10 W. In addition, the combination of AMF HT with MNPs showed a rapid increase in the temperature of the tumor site a few minutes into the procedure (1 and 4 min for RF powers 10 and 5, respectively), and then, the temperature gradually increased during the treatment. Furthermore, the calculated values of computational electromagnetics (CEM) 43 °C for four types of heating protocols in 8 min are reported in Table 2. Also, Table 2 shows the mean of temperature elevation rates for tumoral mice exposed to various RF powers (with or without MNPs) for 8 min. The MNPs showed thermo-sensitizing capability and increased the heating rate of the tumor under different RF powers. The CEM 43 °C values were invalid when the measured temperatures increased to 54 °C, although Juang et al. showed that the reason for this is the occurrence of necrosis in tissues at high temperatures.[20]

Table 2. IR Thermometry of the Tumor to Estimate the Thermal Dose and Temperature Elevation Rate under 8 min AMF Exposure

treatment groups	CEM 43 °C (min)	temperature elevation rate (°C/min)
AMF (5 W)	0.275	0.5
MNPs + AMF (5 W)	41.2	1.25
AMF (10 W)	3.54	0.78
MNPs + AMF (10 W)	not applicable (>1000)	2.5

2.5. Assessment of Therapeutic Efficacy. *2.5.1. MTT Cytotoxicity Assay.* Cytotoxicity of free 5-Fu (Figure 6A) and MNPs (Figure 6B) with/without 5-Fu on the growth of the CT-26 colon cancer cell line was investigated using an MTT

https://doi.org/10.1021/acsomega.1c01763
ACS Omega 2021, 6, 20192−20204

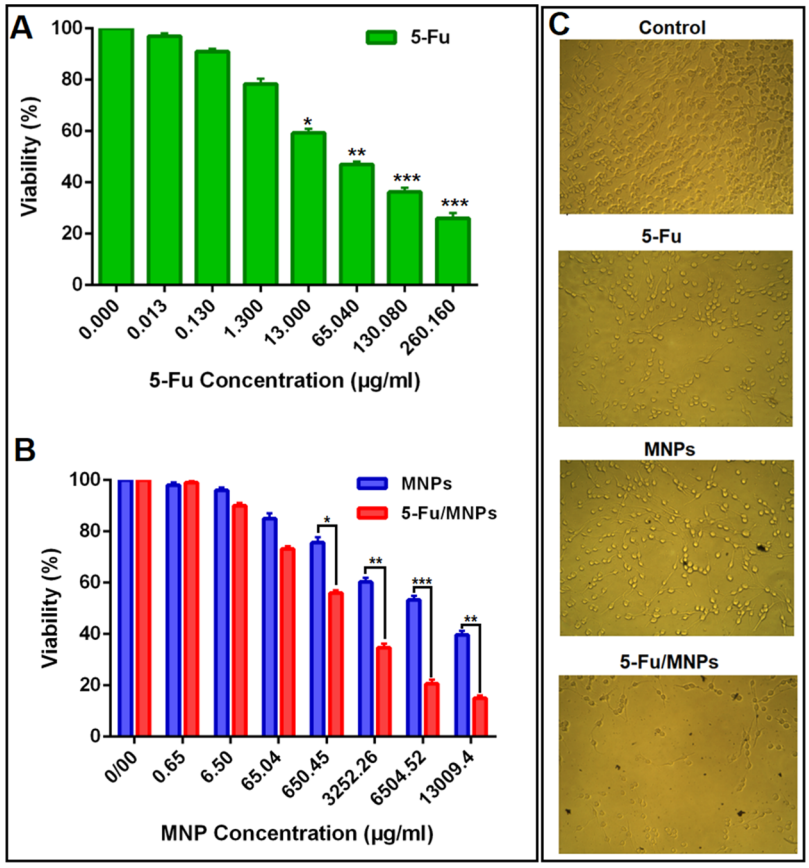

Figure 6. A) MTT assay: the effect of free 5-Fu on the CT-26 cell viability, (B) effect of MNPs and 5-Fu-loaded MNPs on the CT-26 cell viability (all 5-Fu concentrations are equivalent to (A), and (C) optical microscopy images of CT-26 cells after treatment with 130.08 μg/mL concentration of 5-Fu and 6504 μg/mL concentration of MNPs and 5-Fu loaded MNPs for 24 h (containing 130.08 μg/mL of 5-Fu).

assay. Figure 6B illustrates that the viability of CT-26 cells after treatment with MNPs (SPIONs/NGO@PCL−LMWC) even at the highest concentration (0.6 mg/mL) remained above 80% within 24 h. The results suggested that MNPs were biocompatible and only slightly cytotoxic to CT-26 cells, while notable cytotoxicity to the cells was observed with 5-Fu-loaded MNPs, consistent with previous studies.[21] In addition, the figure shows that the IC50 values of 5-Fu, MNPs, and 5-Fu-loaded MNPs were 57.34 ± 0.06, 72.7 ± 0.13, and 25.9 ± 0.05 μg/mL, respectively. Clearly, 5-Fu-loaded MNPs exhibited a 2.21-fold toxicity to CT-26 cells compared to that of free 5-Fu ($P < 0.05$), which may be due to more 5-Fu entering into cells with nanoparticles. Furthermore, optical microscopy images of CT-26 cell viability after treatment with 5-Fu (130.08 μg/mL), MNPs, and 5-Fu/MNPs (6504 μg/mL) are shown in Figure 6C.

2.5.2. Trypan Blue Staining. To verify the biocompatibility of nanoparticles as 5-Fu carriers, immediately after the treatment of the CT-26 cells with 5-Fu (1 μM) or MNPs with/without 5-Fu (equal dose of 5-Fu) alone or combined with AMF HT (13.56 MHz, 50 W, 43 °C), the cells were counted and the cell viability was evaluated through Trypan blue staining. Figure 7A shows the combinatorial effects of 5-Fu, MNPs, and 5-Fu-loaded MNPs alone or in the presence of AMF HT (43 °C) on the CT-26 cell viability. As shown, immediately after the combinatorial treatment on CT-26 cells by 5-Fu, 5-Fu-loaded MNPs, and AMF HT, there was no significant effect on the cell viability in the monolayer culture ($P > 0.05$).

2.5.3. Quantitative Real-Time Polymerase Chain Reaction. Expression of Bax and Bcl-2 genes in CT-26 cells treated with different therapies was evaluated by real-time polymerase chain reaction (PCR). As shown in Figure 7B, except for the nanoparticles and HT groups alone ($P > 0.05$), in the remaining groups, upregulation of the Bax mRNA expression is seen in comparison with that in the control group ($P < 0.01$). Also, therapeutic groups in the presence of AMF HT showed a significant difference in the expression of the Bax gene in comparison with the groups lacking AMF irradiation ($P < 0.01$), which suggests the synergistic effect of a combination therapy of the drug, nanoparticles, and HT. Figure 7C also illustrates a significant reduction in the Bcl-2 gene expression in treatment groups compared to the control ($P < 0.01$), but no significant difference was observed between the control and AMF HT, as well as the control and nanoparticles alone or in combination with the AMF ($P > 0.05$). Studies have shown that increasing the Bax/Bcl-2 mRNA ratio represents the activation of the apoptotic death pathway. Figure 7D illustrates an increase in the Bax/Bcl-2 ratio in the CT-26 cells treated with the combinatorial treatment modality (5-Fu, NPs, 5-Fu loaded NPs, and AMF exposure) compared to that with single-treatment modalities ($P < 0.01$).

2.6. In Vivo Magnetic Drug Targeting and MRI. The magnetically guided targeting ability and MRI results of mice colon cancer in vivo using MNPs were evaluated. As stated before, MRI of the mice bearing the tumor was performed to check for MNP distribution in the tumor area before the injection of MNPs into the tail veins of the mice and 2 h after

https://doi.org/10.1021/acsomega.1c01763
ACS Omega 2021, 6, 20192−20204

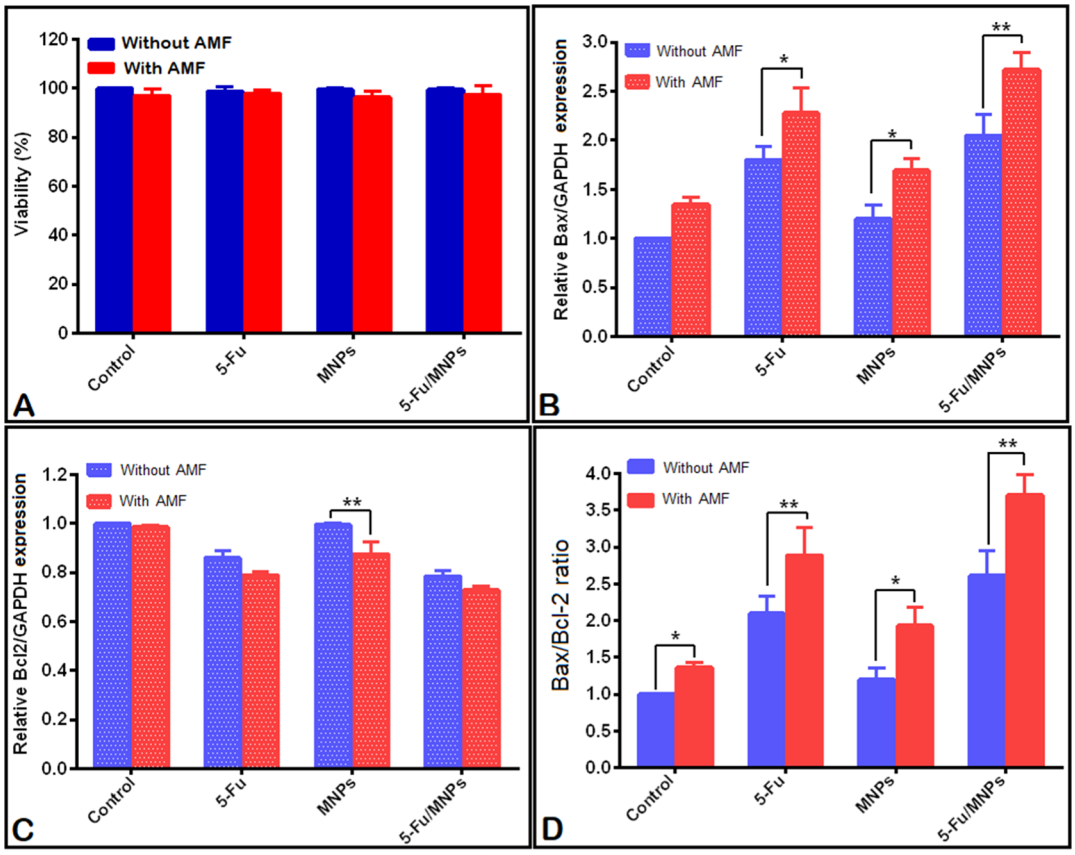

Figure 7. (A) The viability of CT-26 monolayer culture cells was measured using the trypan blue dye exclusion assay method. Effect of 5-Fu, SPION/NGO@PCL−LMWC, and 5-Fu-loaded SPION/NGO@PCL−LMWC alone or in combination with AMF HT (43 °C) on the (B) expression of the Bax gene, (C) expression of the Bcl-2 gene, (D) and the Bax/Bcl-2 mRNA ratio in CT-26 cells. For all experiments, the concentrations of 5-Fu, MNPs, and 5-Fu-loaded MNPs were 0.13, 6.5, and 6.5 μg/mL, respectively. Also, the AMF was applied for 6 min for the nanoparticles group and 17 min for the control groups [mean ± standard deviation (SD), $n = 3$]. Statistical significance is shown as $^{*}P < 0.05$, and $^{**}P < 0.01$, respectively.

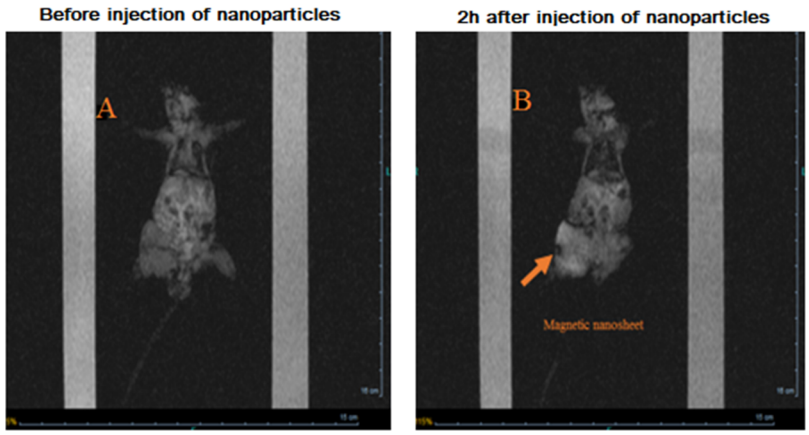

Figure 8. MRI images of CT-26 colorectal-bearing mice injected with 5-Fu-loaded MNPs (10 mg/kg, contain 2.5 mg/kg Fe). (A) MRI coronal images before the injection of MNPs and (B) 2 h after the injection of MNPs. Orange arrow circle shows the MNP accumulation points as a "dark" core at the T2*-weighted scan.

the magnetic targeting. Figure 8A exhibits the MRI initial scans of the mice before the injection of nanoparticles. Scans represent the uniformity of the image intensity in the tumor, which indicates the absence of MNPs. Later, MNPs were injected and guided via a permanent magnetic field and then immobilized into the tumor as seen using the dark areas (Figure 8B), which indicated a successful targeted delivery of MNPs to the tumor site. The results showed that the relative signal enhancement at 24 h was approximately 1.14-fold higher than that in the MNPs group (Figure 8B). As a result, the application of an external permanent magnet caused a significant MRI signal change in colorectal BALB/c mice tumors 2 h after MNP administration. In fact, MNPs were injected intravenously to make clearer the effect of the magnet positioned on the tumor. However, application of an external magnetic field for drug targeting has several limitations, such as

https://doi.org/10.1021/acsomega.1c01763
ACS Omega 2021, 6, 20192−20204

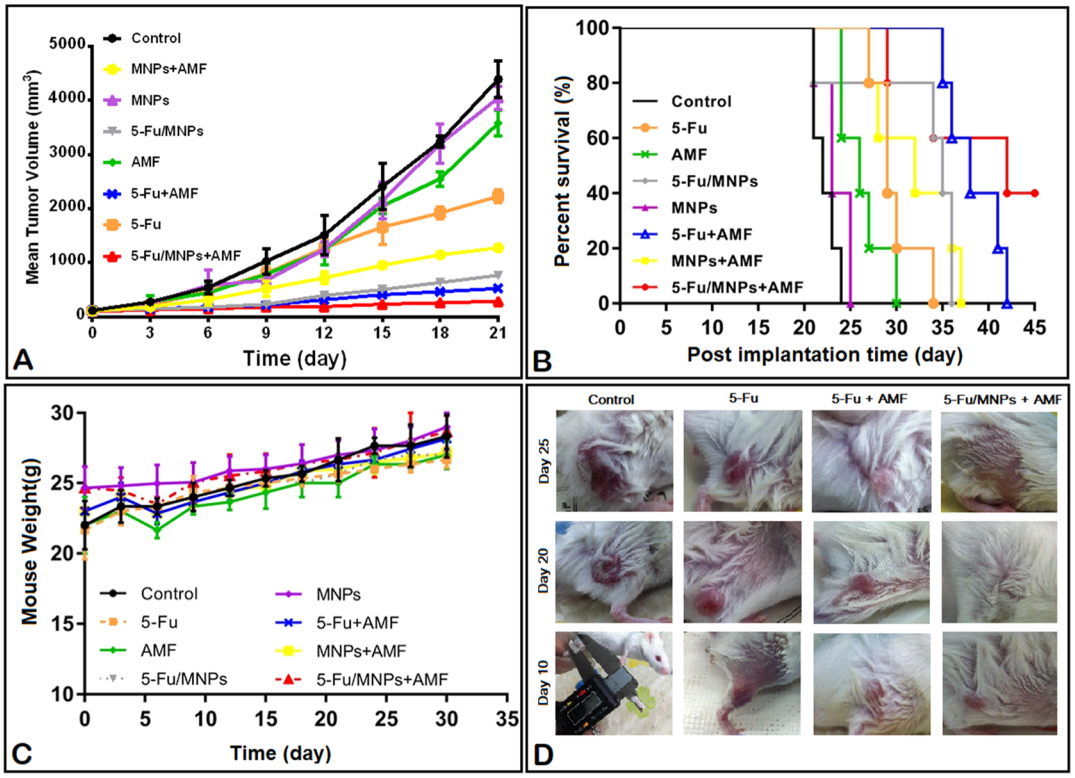

Figure 9. Antitumor efficacy of free 5-Fu and 5-Fu-loaded MNPs with or without AMF HT were determined in the CT-26 colorectal tumor model. (A) Colon tumor volume in different therapeutic groups on the 21st day, (B) Kaplan–Meier plot, (C) body weight changes, and (D) photographs of mice in control and treated groups. (Mean ± SD, n = 5).

Table 3. Tumor Growth Inhibition and Survival Time Data of CT-26 Colorectal-Bearing BALB/c Mice (n = 5) after Different Treatment Modalities

	tumor growth inhibition			survival time		
treatment groups	median tumor volume (mm^3)	mean growth inhibition rate (%)	P value	median life (day)	increase in life span (%)	P value
control	4394.01			22		
5-Fu	2229.6	49.25	<0.001	29	31.81	0.004
MNPs	4144.45	7.9	NS	23	4.54	NS
5-Fu/MNPs	766.51	82.55	<0.001	35	59.09	<0.001
AMF	3580.07	18.52	0.019	26	18.18	0.017
5-Fu + AMF	523.88	88.07	<0.001	38	72.72	<0.001
MNPs + AMF	1276.93	70.93	<0.001	32	45.45	<0.001
5-Fu/MNPs + AMF	285.08	93.51	<0.001	42	90.9	<0.001

the strength and spatial geometry of the magnetic field with respect to the target site that can be localized by nanoparticles at any depth within the tissue.[22]

2.7. Assessment of Therapeutic Efficacy. The antitumor effect of 5-Fu-loaded MNPs under AMF exposure (13.56 MHz, 5 W) was evaluated in colon cancer by tumor volume, survival time, and body weight changes. After treating the mice with saline, free 5-Fu, MNPs, 5-Fu-loaded MNPs, AMF (5 W, 18 min), 5-Fu + AMF, MNPs + AMF (5 W, 4 min), and 5-Fu-loaded MNPs + AMF, median tumor volumes (n = 5) on the 21st day post-subcutaneous tumor implantation were reported to be 4394.01, 2229.6, 4144.45, 766.51, 3580.07, 523.88, 1276.93, and 285.08 mm^3, respectively (Figure 9A, Table 3). Both 5-Fu and AMF alone significantly inhibited tumor growth (P < 0.01), while MNPs had no significant antitumor effect (P > 0.05). The 5-Fu + AMF group also showed a significant reduction in the tumor volume on day 21 (P < 0.05), whereas, as shown in the survival results (Figure 9B), mice in this group died after the recurrence of the tumor during 42 days. This may be due to the short half-life of the drug in the body. Post hoc analysis confirmed that 5-Fu-loaded MNPs in the presence of AMF exhibited the strongest antitumor effect on colon cancer compared to the other treatment groups (P < 0.001, Figure 9A). The results demonstrated that the RF HT increased the therapeutic efficiency of the drug and nanoparticles (P < 0.001). We also evaluated the survival time of mice with colon cancer. After treatment with different modalities, the median survival time is illustrated (Figure 9B, Table 3). The order of the median survival time of mice was as follows: 5-Fu-loaded MNPs + AMF (42 day) > 5-Fu + AMF (38 day) > 5-Fu-loaded MNPs (35 day) > MNPs + AMF (32 day) > 5-Fu (29 day) > AMF (26 day) > MNPs (23 day) > saline (22 day). The median survival time of 5-Fu-loaded MNPs exposed to the AMF was significantly prolonged compared to the rest (P < 0.05, Figure 9B). Also, we examined the effects of various therapeutic approaches on body weight

https://doi.org/10.1021/acsomega.1c01763
ACS Omega 2021, 6, 20192−20204

changes in tumor-bearing mice. It has been clearly recognized that animals lose their body weight during toxic treatments methods. The body weight of mice treated in all treatment groups slightly increased in a manner similar to that of the normal mice as the control (Figure 9C), which indicates that the mice matured without any significant toxic effects. In addition, changes in the mice tumor volume in the treatment groups are presented qualitatively in Figure 9D.

3. DISCUSSION

One of the major challenges in treating colon cancer is how to improve the local accumulation of anticancer drugs in the tumor sites and prevent the accumulation in healthy tissues.[23] MNPs as a platform for drug targeting offer a new opportunity for localized cancer treatment.[24] The main purpose of the current study was to investigate the treatment efficiency of the oncothermia method by AMF in the presence of drug-carrying MNPs in colon cancer in vitro and in vivo.

As shown in Figure 3 and Table 1, the synthesized 5-Fu-loaded superparamagnetic graphene oxide nanoparticles had a size below 80 nm and a surface charge of −30 mV. Generally, the size of 10−100 nm is considered to be the optimum size for nanocarriers.[25,26] The zeta potential quantity indicates an index for particle stability. The absolute zeta potential value of more than 30 mV represents physical stability,[27] which can create strong repulsive forces between NPs to prevent particles from aggregating in a solution.

In this study, when 5-Fu was loaded onto MNPs, a slow release of 5-Fu was observed at 37 °C. The results showed that heating at 43 °C had a significant effect on the 5-Fu release rate compared to that at 37 °C (Figure 4A). This is one of the great advantages of heat-sensitive MNPs, that their drug release is easily regulated by remote control. Furthermore, 5-Fu-loading on SPIONs/NGO@PCL−LMWC showed a greater inhibitory effect on CT-26 cell growth than 5-Fu. The results demonstrate that the cytotoxicity of 5-Fu loaded MNPs was concentration-dependent and increased with the increase in the concentration of MNPs from 0.13 to 260 μg/mL. The evaluation of the toxicity of MNPs showed no significant toxicity at the highest concentration (0.6 mg/mL), and the cell viability was above 80% (Figure 6).

The CT-26 cell treatment efficiencies of various treatments methods were evaluated using real-time PCR. The results demonstrated that 5-Fu, MNPs, and 5-Fu loaded MNPs could be more toxic than the single-treatment method if combined with AMF HT (Figure 7). These results also demonstrated the significant difference in the Bax/Bcl-2 mRNA ratio between free 5-Fu and 5-Fu-loaded nanoparticles groups ($P < 0.05$, Figure 7D), which indicates that drug absorption by cells increases with drug loading in nanoparticles. The obtained results illustrated that the cytotoxicity of 5-Fu was significantly enhanced in the presence of AMF HT (Figure 7) and this could be because heat increases the permeability of the cell membrane to chemotherapeutic agents. Magnetite NGO is used to convert RF waves to vibrational energy in order to generate heat for cancer cell killing.[28] Gannon et al. reported that a combination of single-wall carbon nanotubes and RF produces lethal thermal effects, which causes damage to the malignant cells.[5]

To assess whether the designed 5-Fu loaded MNPs could be delivered to the colorectal tumor site by a magnetic field, the MNP tracking was evaluated using MRI (Figure 8). The distribution of MNPs in the tumor area indicated that MNPs were successfully delivered to the tumor by magnetic drug targeting (Figure 8). The results of measuring the temperature changes with the IR camera showed a wide range of temperatures above 37 °C on the skin surface of the colon tumor, which was similar to the results reported by Alphandéry et al.[29] The increase in the temperature during the first few minutes of exposure to AMF was very intense, and then, the temperature reached an equilibrium (Figure 5C and Table 2) because heat transmission parameters (convection and conduction) were attained.[30] Based on the results shown in Figure 9A and Table 3, the AMF (5 W, 18 min) had an inhibition tumor growth rate of 18.52% and increased the life time of the mice bearing the tumor by 18.18%. It was not significant compared to that with AMF combined with MNPs or the drug. Basel et al. demonstrated that the body is extremely permeable to the AMF, which itself produces no known effects in the mice.[31] HT with the AMF (5 W, 4 min) combined with MNPs increased the inhibition tumor growth and life span rate to 70.93% and 45.45%, respectively (Table 3). Furthermore, the results showed that the AMF (5 W, 18 min) combined with 5-Fu MNPs increased the inhibition tumor growth rate to 88.07% and the life time by 72.72% (Table 3). The 5-Fu anticancer effects when exposed to AMF compared to that of free 5-Fu could be attributed to the fact that HT with the AMF can increase the drug release and uptake rate of the tumor by macroscopic mechanisms of macromolecular massage of the cell membrane. The targeting of drug delivery by the AMF is based on strain/stress that can increase the drug level inside the cancer cells and cause the cells to be thermally or mechanically killed.[32,33] According to the results shown in Table 3, 5-Fu-loaded MNPs can inhibit or delay the growth of the tumor more effectively than free 5-Fu. Improving the anti-cancer effect of 5-Fu-loaded nanoparticles compared to that of free 5-Fu can be due to the sustained release and a prolonged half-life of 5-Fu in the blood circulation.[34] In addition, the results indicated that tumor-bearing CT-26 mice treated with 5-Fu loaded MNPs in combination with the AMF (5 W, 4 min) had the strongest inhibitory effect (93.51%) and the highest survival time (90.9%, 42 day) compared to those of the control group (Figure 9A−C, Table 3). This enhanced antitumor effect can be attributed to several parameters related to the concomitant effects of chemotherapy and HT, including the increased blood flow and membrane permeability under the increased temperature, which causes an increased drug concentration in the tumor.[35]

4. CONCLUSIONS

According to this study, SPION/NGO@PCL−LMWC NPs as 5-Fu carriers are a promising cancer treatment modality, and by applying AMF HT, the cytotoxic effects of MNPs are increased. Also, we demonstrated that the combination of HT with MNPs significantly affected the temperature profile of CT-26 tumors. HT−AMF would be quite useful when a targeted drug delivery method is developed to concentrate nanoparticles specifically in the tumor in order to ignore the AMF's thermal side effects. The results clearly support the concept that the use of active targeting by an external magnetic field after the intravenous injection of MNPs and exposing the tumor with the AMF can be an effective strategy to increase the therapeutic efficiency. Such approaches ultimately lead to an effective reduction in the dose of anticancer drugs, reduce

https://doi.org/10.1021/acsomega.1c01763
ACS Omega 2021, 6, 20192−20204

the systemic toxicity, and increase the efficiency of nano-HT by concentrating nanoparticles in the tumor site and local HT.

5. MATERIALS AND METHODS

5.1. Materials. 5-Fu, potassium permanganate (KM_nO_4), phosphoric acid (H_3PO_4), *N*,*N*′-dicyclohexylcarbodiimide (DCC), graphite powder, 4-dimethylaminopyridine (DMAP), potassium ferrocyanide(II) trihydrate ($K_4[Fe(CN)_6]\cdot 3H_2O$), hydrochloric acid (HCl), and formaldehyde (CH_2O) solution were obtained from Sigma (St Louis, USA). Ferrous chloride ($FeCl_2\cdot 4H_2O$), ferric chloride ($FeCl_3\cdot 6H_2O$), 1-ethyl-3-(3-dimethylaminopropyl)carbodiimide (EDC), LMWC, PCL, dimethylformamide (DMF), *N*-hydroxysuccinimide (NHS), ammonia solution (25 vol %), dichloromethane, hydrogen peroxide (H_2O_2), Span60, and Tween60 were obtained from Merck (Darmstadt, Germany). Roswell Park Memorial Institute (RPMI) 1640 culture medium, fetal bovine serum, and trypsin−ethylenediamine tetraacetic acid were provided from Biowest (Spain). The CT-26 (mouse colon cancer) cell line was purchased from the Pasteur Institute of Iran.

5.2. Preparation of Drug-Loaded SPIO/NGO@PCL−LMWC Nanocarriers. *5.2.1. Step 1: Synthesis of NGO Nanosheets.* NGO was synthesized through the improved Hummer's method.[36] Briefly, 1 g of graphite powder was added to a 200 mL sulfuric and phosphoric acid solution with a 9:1 vol/vol ratio. Afterward, $KMnO_4$ (6 g) was mixed in the solution and stirred for 72 h at 50 °C. The solution was poured into a container of ice water, and then, H_2O_2 (4 mL) was added dropwise to the mixture until its color changed to brownish yellow. The resultant GO was centrifuged and then washed twice with HCl (10%) and deionized water (DW) separately. Finally, the graphite oxide solution was dried in an oven at 40 °C.

5.2.2. Step 2: Synthesis of SPIO/NGO Nanoparticles. $FeCl_2\cdot 4H_2O$ (1 g) and $FeCl_3\cdot 6H_2O$ (2.6 g) were dissolved in DW (50 mL) containing 250 mg of GO under a nitrogen atmosphere. Moreover, an ammonia solution (10 mL, 25%) was added to the medium, and it was stirred at 70 °C for 2 h. Finally, the SPION/NGO product was separated magnetically and washed with DW and ethanol two−three times.[37]

5.2.3. Step 3: Synthesis of SPIO/NGO@PCL Nanoparticles. In this section, 10 mg of SPIO/NGO nanoparticles was dispersed in DMF (10 mL); afterward, 20 mg of PCL was added to the mixture, followed by stirring for 1 h. Then, DCC (4 mg) and DMAP (1 mg) were mixed in the solution, and the reaction was continued at room temperature for 4 h. The obtained product was centrifuged and washed with DMF thrice, and then, it was dried at 40 °C.

5.2.4. Step 4: Synthesis of SPIO/NGO@PCL−LMWC Nanoparticles. In order to functionalize with LMWC, 10 mg of SPIO/NGO@PCL nanoparticles synthesized in the previous section was dispersed in 10 mL of PBS with the pH value of 7.4 by an ultrasound instrument (power of 50 W for 20 min). Furthermore, 30 mg of EDC and 20 mg of NHS were slowly mixed into the solution (for 20 min), followed by stirring the dispersion for 2 h. Subsequently, 50 mg of LMWC was added to the solution and stirred for 24 h. SPION/NGO@PCL−LMWC nanoparticles were collected with centrifugation, followed by being washed twice with DW, and then, the product was dried at 40 °C for 24 h.

5.3. Preparation of Drug-Loaded Nanoparticles. To prepare 5-Fu loaded nanoparticles, 10 mg of SPIO/NGO@PCL−LMWC was dispersed in DW (10 mL). After, 5-Fu (1 mg) was added to the dispersion medium. The mixture was stirred magnetically (400 rpm) at room temperature for 48 h. The obtained nanoparticles were separated by centrifugation and washed once with DW to remove unloaded 5-Fu. Eventually, the nanoparticles were freeze-dried and stored at 4 °C. The schematic diagram of the final nanoparticle structure is shown in Figure 1.

5.4. Characterization of Nanoparticles. A Bruker EQUINOX 55 FT-IR apparatus was used in the ATR mode to characterize the nanoparticles. The morphological characteristics of 5-Fu-loaded SPION/NGO@PCL−LMWC was analyzed by TEM. The size and surface charge of nanoparticles were measured in DW through dynamic light scattering and a Zetasizer (Brookhaven Instruments, USA). Furthermore, XRD patterns of the nanoparticles were obtained using an X-ray diffractometer with Cu Kα radiation (X'Pert PRO MPD, PANalytical Company, Netherlands). The polymer content on the surface of nanoparticles was determined by TGA. The sample was heated from room temperature to 600 °C (a rate of 20 °C/min) under a nitrogen atmosphere.

5.5. Drug Content and Encapsulation Efficiency of Nanoparticles. The concentration of 5-Fu in a nanoparticle was determined by a UV spectrophotometer (Pharmacia Biotech, United State of America). 5-Fu/MNPs were dissolved in acetone. Then, the suspended magnetite particles were separated by magnets. These steps were done on nanoparticles without the drug, and these samples were used as blanks in the absorbance measurement. Eventually, the 5-Fu concentration in the solution was assessed at a wavelength of 265 nm. Drug loading content and encapsulation efficiency were calculated using the following equations

$$\text{drug loading content (\%)} = \frac{\text{weight of drug in nanoparticles}}{\text{weight of nanoparticles}} \times 100 \quad (1)$$

$$\text{encapsulation efficiency (\%)} = \frac{\text{weight of drug in nanoparticles}}{\text{weight of feeding drug}} \times 100 \quad (2)$$

In addition, experimental studies of the 5-Fu release from MNPs in the in vitro condition were carried out using the diffusion method at various temperatures (37 and 43 °C).

5.6. In Vitro Experiments. *5.6.1. Cellular Uptake of Nanoparticles.* The cellular uptake of MNPs was assessed by Prussian blue staining. CT-26 cells were cultured in 6-well plates (SPL) containing complete RPMI-1640 culture medium and incubated in CO_2 (5%) at 37 °C for 24 h. Then, the medium was changed, and the cells were incubated for another 24 h with 5-Fu/SPION/NGO@PCL−LMWC NPs at the concentration of Fe_3O_4 (11.8 μg/mL). After being kept overnight, the medium was removed and the cells were fixed with a formaldehyde solution (4%) for 20 min. Then, the cells were stained with a Prussian blue solution containing equal volumes of 2% potassium ferrocyanide(II) trihydrate and 2% hydrochloric acid. Finally, the result was determined by light microscopy (Bell, Italy).

5.7. Cytotoxicity Analysis. *5.7.1. MTT Assay.* CT-26 cells were seeded into 96-well plates (5×10^4 cells/well) containing 100 μL of the complete culture medium and left to grow for 24 h. Eight different doses (0, 0.01, 0.1, 1, 10, 100, 1000, and 2000 μM) of free 5-Fu, MNPs, or 5-Fu-loaded MNPs were added to

https://doi.org/10.1021/acsomega.1c01763
ACS Omega 2021, 6, 20192−20204

Table 4. Primer Sequences of the Genes Used for Real-Time PCR Experiments

genes	forward primers	reverse primer
Bax	5′-CGATGAACTGGACAACAACATGG-3′	5′-GCAAAGTAGAAAAGGGCAACCAC-3′
Bcl-2	5′-AGGATTGTGGCCTTCTTTGAGTT-3′	5′-GCCGGTTCAGGTACTCAGTCAT-3′
GAPDH	5′-AGTTCAACGGCACAGTCAAG-3′	5′-TACTCAGCACCAGCATCACC-3′

the medium during the first 24 h. Then, the RPMI-1640 medium was removed, the cells were washed with PBS, and the MTT solution (5 mg/mL in PBS) was added to the cells. The cells were incubated for 4 h in a dark environment at 37 °C. After that, the MTT was removed, the dimethyl sulfoxide solution (100 μL/well) was added to the cells, and the plate was placed on a shaker for 30 min. Ultimately, the optical density was read at 540 nm.

5.7.2. AMF Hyperthermia. A high-frequency generator manufactured by the Sharif University of IRAN was used to induce an alternating current (40 A/m and a frequency of 13.56 MHz). The current passed through a custom-made four-turn water-cooled copper coil with an internal diameter of 40 mm. CT-26 cells (5×10^5) were cultured in flasks overnight. Then, the cells were treated with 1 μM 5-Fu (0.13 μg/mL), 6.5 μg/mL 5-Fu/MNPs (containing 1 μM of 5-Fu), and 6.5 μg/mL SPION/NGO@PCL−LMWC nanoparticles for 24 h. Control and treated groups were irradiated with AMF (power of 50 W) to obtain a temperature of 43 °C (6 and 17 min exposure for nanoparticles and control groups, respectively). After treatment, the CT-26 cells were counted and assessed for survival by using the trypan blue dye and real-time PCR assays. During treatment, cell temperature changes were evaluated using an IR thermal camera (Testo 875-1i, Germany) during AMF radiation.

5.7.3. Viability Assay. After treatment, suspensions of control and treated cells were stained by a trypan blue dye. The cell suspensions were examined by an optical microscope, and blue-colored cells were considered as dead cells.

5.7.4. Real-Time PCR. Pro-apoptotic and anti-apoptotic effects of 5-Fu (0.13 μg/mL) and 5-Fu-loaded SPION/NGO@PCL−LMWC (6.5 μg/mL) alone or combined with RF HT (43 °C) were studied with the evaluation of Bax and Bcl-2 gene expression. To this end, the total RNA of the treated CT-26 cells was extracted by RNX-plus (CinnaGen, Iran). RNA concentration was evaluated by measuring the optical spectrum at 260 nm, and the absorbance ratio 260 nm/280 nm confirmed purity. Then, from the total RNA extracted (3 μg), according to the manufacturer of the cDNA kit (Takara Bio Inc., Japan), cDNA was obtained. Real-time PCR was carried out by a SYBR Green qPCR master mix kit (Takara Bio Inc., Japan). Real-time PCR was performed under the following conditions for up to 40 cycles: (1) initial activation (95 °C, 10 min), (2) denaturation (95 °C, 15 s), (3) annealing (55 °C, 20 s), and (4) extension (72 °C, 15 s). Results were normalized to GAPDH as the housekeeping gene and analyzed with DataAssist (v3.01) software. The primer sequences used are listed in Table 4.

5.8. In Vivo Experiments. *5.8.1. Mouse Models of Colon Cancer.* BALB/c mice (20−30 g) were purchased from the Pasteur Institute of Tehran, Iran. Animals were kept under the standard conditions in accordance with the Helsinki Declaration at the Animal Research Center of Iran University of Medical Sciences (Tehran, Iran). Mice were housed under standard laboratory conditions (a 12 h light/dark cycling), and animals were allowed to have free access to standard food and water. For mice modeling of colon cancer, CT-26 cell suspensions in RPMI-1640 medium (2×10^6/100 μL) were injected subcutaneously into the right leg of the mice. Animals were monitored and weighed each day. Euthanasia was performed by CO_2 asphyxiation or cervical dislocation, with or without prior cardiac puncture.

5.8.2. Magnetic Resonance Imaging. On the 14th day post-subcutaneous tumor implantation, 5-Fu-loaded MNPs were injected into the tail vein of mice with a dose of 10 mg/kg (containing 2.5 mg/kg Fe), and then, the mice were retained in the magnetic field for 2 h. To evaluate colorectal-magnetic-targeting ability of nanoparticles, the mice were imaged with MRI (T2-weighted images) before the injection of MNPs and after the magnetic targeting. All MRI images were obtained on a 3 T MRI scanner (Siemens, Germany) using the surface coil. To quantify the contrast enhancement, the signal-to-noise ratio (SNR) within the regions of interest of the images was calculated according to the following formula

$$\Delta\mathrm{SNR} = (|\mathrm{SNRpost} - \mathrm{SNRprel})/\mathrm{SNRpre}$$

where SNRpre is the signal intensity of the tumor before the injection of the MNPs and SNRpost is the signal intensity of the tumor after MNP injection.

5.8.3. AMF and Thermometry. The mice were placed into an alternating magnetic coil, and an AMF was applied at a field strength of 40 A/m and a frequency of 13.56 MHz to the mice injected with and without MNPs. We monitored the temperature within the tumor area and surrounding normal area by IR thermal imaging using a Testo IR camera (875-2i, United Kingdom https://www.testo.com/en-UK/parameters/thermal-imaging-cameras/c/parameters_thermal_imager) in real time in AMF application. The temperature of the heated area was determined by taking photographic images of the tumor area during the AMF exposure time using a Testo 875 thermal imager combined with high IR resolution.

5.8.4. Thermal Dose Calculation. Sapareto and Dewey proposed the Arrhenius model for calculating the thermal dose of hyperthermic treatments.[38] The following equation allows the time−temperature data to be converted to an equivalent amount of heating minutes at 43 °C (CEM 43 °C) using eq 3. The thermal dose is calculated as

$$\mathrm{CEM}\ 43\ ^\circ\mathrm{C} = \sum_{i=1}^{n} t_i \cdot R^{(43-T_m)}$$

$$\text{that } R = \begin{cases} 0.25 & T_m \le 43\ ^\circ\mathrm{C} \\ 0.5 & T_m > 43\ ^\circ\mathrm{C} \end{cases} \quad (3)$$

where t_i, T_m, and R in the above equation are the i-th time interval of the treatment, the average temperature during the desired heating period, and a constant equal to 0.5 and 0.25 when $T > 43$ °C and $T < 43$ °C, respectively.

5.8.5. In Vivo Antitumor Efficacy. A total of 40 (20−30 g) BALB/c mice were prepared. After the implantation of tumor CT-26 cells in mice, we waited for about 10−12 days and allowed the tumor to grow until its volume reached 50−100

https://doi.org/10.1021/acsomega.1c01763
ACS Omega 2021, 6, 20192−20204

mm^3. These 40 mice were randomly divided into two categories and eight groups (n = 5). Tumor-bearing mice in the first category did not receive any AMF; whereas those in the second category were put into the AMF (40 A/m; 13.56 MHz) on day 16.

The first category consisted of four groups: group 1: normal saline (sham); group 2: 5-Fu solution alone; group 3: SPION−NGO@PCL−LMWC (MNPs) and the Nd−Fe−B magnet for 2 h; and group 4: 5-Fu-loaded MNPs and the Nd−Fe−B magnet for 2 h (only groups that received MNPs were exposed to the magnetic field). The second category (with AMF) also consisted of four groups: group 5: normal saline (AMF exposure time: 18 min); group 6: 5-Fu solution (AMF exposure time: 18 min); group 7: MNPs and the Nd−Fe−B magnet (after 2 h, AMF exposure time: 4 min); and group 8: 5-Fu-loaded MNPs and the Nd−Fe−B magnet (after 2 h, AMF exposure time: 4 min). In both categories, mice were treated with 5-Fu and MNP injections through the tail vein each day for the first 5 days (12−16 days) of the experiment with 5-Fu (1 mg/kg) and MNPs (50 mg/kg containing 1 mg/kg of 5-Fu), respectively. In the second category, all mice were put into the alternating current magnetic coil on day 16. Following the treatment, the size of the tumor was measured by a digital caliper every 3 days, and the tumor volume was calculated by eq 4

$$V = \frac{\text{width}^2}{2} \times \text{length} \quad (4)$$

5.8.6. Body Weight and Survival Assessment. The body weight losses and surviving times were evaluated after the treatment procedure was carried out. The body weight changes of the mice in each group were measured twice per week for 1 month. Survival was monitored daily and analyzed by the Kaplan−Meier survival curves.

5.9. Statistical Analysis. Tumor growth inhibitory effects of 5-Fu-loaded MNPs on five mice per group were studied. All data are displayed as mean ± SD. Statistical analysis using one-way ANOVA was performed using GraphPad Prism 6. *P*-values less than 0.05 were considered to be statistically significant.

AUTHOR INFORMATION

Corresponding Author

Samideh Khoei − *Finetech in Medicine Research Centre, Iran University of Medical Sciences, Tehran 1449614535, Iran; Department of Medical Physics, School of Medicine, Iran University of Medical Sciences, Tehran 1449614535, Iran;* orcid.org/0000-0001-9357-0229; Phone: (0098) 21 88622647; Email: khoei.s@iums.ac.ir, skhoei@gmail.com; Fax: (0098) 21 88622647

Authors

Leila Kiamohammadi − *Department of Medical Physics, School of Medicine, Iran University of Medical Sciences, Tehran 1449614535, Iran*

Leili Asadi − *Department of Medical Physics, School of Medicine, Iran University of Medical Sciences, Tehran 1449614535, Iran*

Sakine Shirvalilou − *Finetech in Medicine Research Centre, Iran University of Medical Sciences, Tehran 1449614535, Iran;* orcid.org/0000-0003-3213-8824

Sepideh Khoee − *Department of Polymer Chemistry, School of Chemistry, College of Science, University of Tehran, Tehran 14155 6455, Iran;* orcid.org/0000-0001-7297-8743

Maryam Soleymani − *Department of Polymer Chemistry, School of Chemistry, College of Science, University of Tehran, Tehran 14155 6455, Iran*

Soraya Emamgholizadeh Minaei − *Department of Medical Physics and Imaging, Urmia University of Medical Sciences, Urmia 571478334, Iran*

Complete contact information is available at: https://pubs.acs.org/10.1021/acsomega.1c01763

Author Contributions

All authors contributed to the study conception and design. Sepideh Khoee, M.S., and S.E.M. contributed to material preparation. L.K., L.A., and S.S. conducted animal studies, experiments, took photos (MRI and IR camera), and collected data. The project was supervised and guided by Samideh Khoei.

Notes

The authors declare no competing financial interest.
This research was approved by the Ethics Committee of Iran University of Medical Sciences.

ACKNOWLEDGMENTS

Financial support by grant no. 27726 received from the School of Medicine, Iran University of Medical Sciences (IUMS), is acknowledged.

REFERENCES

(1) Chen, L.; Wu, Y.; Wu, H.; Li, J.; Xie, J.; Zang, F.; Ma, M.; Gu, N.; Zhang, Y. Magnetic targeting combined with active targeting of dual-ligand iron oxide nanoprobes to promote the penetration depth in tumors for effective magnetic resonance imaging and hyperthermia. *Acta Biomater.* **2019**, *96*, 491−504.

(2) Chen, L.; Chen, C.; Wang, P.; Chen, C.; Wu, L.-F.; Song, T. A compound magnetic field generating system for targeted killing of Staphylococcus aureus by magnetotactic bacteria in a microfluidic chip. *J. Magn. Magn. Mater.* **2017**, *427*, 90−94.

(3) Afzalipour, R.; Khoei, S.; Khoee, S.; Shirvalilou, S.; Raoufi, N. J.; Motevalian, M.; Karimi, M. Y. Thermosensitive magnetic nanoparticles exposed to alternating magnetic field and heat-mediated chemotherapy for an effective dual therapy in rat glioma model. *Nanomed. Nanotech. Biol. Med.* **2021**, *31*, 102319.

(4) Su, Z.; Liu, D.; Chen, L.; Zhang, J.; Ru, L.; Chen, Z.; Gao, Z.; Wang, X. CD44-targeted magnetic nanoparticles kill head and neck squamous cell carcinoma stem cells in an alternating magnetic field. *Int. J. Nanomed.* **2019**, *14*, 7549.

(5) Gannon, C. J.; Cherukuri, P.; Yakobson, B. I.; Cognet, L.; Kanzius, J. S.; Kittrell, C.; Weisman, R. B.; Pasquali, M.; Schmidt, H. K.; Smalley, R. E.; Curley, S. A. Carbon nanotube-enhanced thermal destruction of cancer cells in a noninvasive radiofrequency field. *Cancer* **2007**, *110*, 2654−2665.

(6) Singh, A.; Jain, S.; Sahoo, S. K. Magnetic nanoparticles for amalgamation of magnetic hyperthermia and chemotherapy: An approach towards enhanced attenuation of tumor. *Mater. Sci. Eng. C* **2020**, *110*, 110695.

(7) Shirvalilou, S.; Khoei, S.; Khoee, S.; Mahdavi, S. R.; Raoufi, N. J.; Motevalian, M.; Karimi, M. Y. Enhancement radiation-induced apoptosis in C6 glioma tumor-bearing rats via pH-responsive magnetic graphene oxide nanocarrier. *J. Photochem. Photobiol., B* **2020**, *205*, 111827.

(8) Hervault, A.; Thanh, N. T. K. Magnetic nanoparticle-based therapeutic agents for thermo-chemotherapy treatment of cancer. *Nanoscale* **2014**, *6*, 11553−11573.

(9) Sugumaran, P. J.; Liu, X.-L.; Herng, T. S.; Peng, E.; Ding, J. GO-functionalized large magnetic iron oxide nanoparticles with enhanced colloidal stability and hyperthermia performance. *ACS Appl. Mater. Interfaces* **2019**, *11*, 22703−22713.

(10) Nemati, Z.; Salili, S. M.; Alonso, J.; Ataie, A.; Das, R.; Phan, M. H.; Srikanth, H. Superparamagnetic iron oxide nanodiscs for hyperthermia therapy: Does size matter? *J. Alloys Compd.* **2017**, *714*, 709−714.
(11) Mahmoudi, M.; Sant, S.; Wang, B.; Laurent, S.; Sen, T. Superparamagnetic iron oxide nanoparticles (SPIONs): development, surface modification and applications in chemotherapy. *Adv. Drug Delivery Rev.* **2011**, *63*, 24−46.
(12) Cho, M.; Cervadoro, A.; Ramirez, M.; Stigliano, C.; Brazdeikis, A.; Colvin, V.; Civera, P.; Key, J.; Decuzzi, P. Assembly of iron oxide nanocubes for enhanced cancer hyperthermia and magnetic resonance imaging. *Nanomaterial* **2017**, *7*, 72.
(13) Rajaee, Z.; Khoei, S.; Mahdavi, S. R.; Ebrahimi, M.; Shirvalilou, S.; Mahdavian, A. Evaluation of the effect of hyperthermia and electron radiation on prostate cancer stem cells. *Radiat. Environ. Biophys.* **2018**, *57*, 133−142.
(14) Al-Ahmady, Z. S.; Al-Jamal, W. T.; Bossche, J. V.; Bui, T. T.; Drake, A. F.; Mason, A. J.; Kostarelos, K. Lipid−peptide vesicle nanoscale hybrids for triggered drug release by mild hyperthermia in vitro and in vivo. *ACS Nano* **2012**, *6*, 9335−9346.
(15) Castellanos-Rubio, I.; Rodrigo, I.; Olazagoitia-Garmendia, A.; Arriortua, O.; Gil de Muro, I.; Garitaonandia, J. S.; Bilbao, J. R.; Fdez-Gubieda, M. L.; Plazaola, F.; Orue, I. Highly Reproducible Hyperthermia Response in Water, Agar and Cellular Environment by Discretely PEGylated Magnetite Nanoparticles. *ACS Appl. Mater. Interfaces* **2020**, *12*, 27917−27929.
(16) Eynali, S.; Khoei, S.; Khoee, S.; Esmaelbeygi, E. Evaluation of the cytotoxic effects of hyperthermia and 5-fluorouracil-loaded magnetic nanoparticles on human colon cancer cell line HT-29. *Int. J. Hyperther.* **2017**, *33*, 327−335.
(17) Zhu, Z.; Cheng, R.; Ling, L.; Li, Q.; Chen, S. Rapid and Large-Scale Production of Multi-Fluorescence Carbon Dots by a Magnetic Hyperthermia Method. *Angew. Chem., Int. Ed.* **2020**, *59*, 3099−3105.
(18) Asadi, L.; Shirvalilou, S.; Khoee, S.; Khoei, S. Cytotoxic effect of 5-Fluorouracil-loaded polymer-coated magnetite nanographene oxide combined with radiofrequency. *Anti-Cancer Agents Med. Chem.* **2018**, *18*, 1148−1155.
(19) Beola, L.; Asín, L.; Roma-Rodrigues, C.; Fernández-Afonso, Y.; Fratila, R. M.; Serantes, D.; Ruta, S.; Chantrell, R. W.; Fernandes, A. R.; Baptista, P. V.; de la Fuente, J. M.; Grazú, V.; Gutiérrez, L. The Intracellular Number of Magnetic Nanoparticles Modulates the Apoptotic Death Pathway after Magnetic Hyperthermia Treatment. *ACS Appl. Mater. Interfaces* **2020**, *12*, 43474−43487.
(20) Juang, T.; Stauffer, P. R.; Craciunescu, O. A.; Maccarini, P. F.; Yuan, Y.; Das, S. K.; Dewhirst, M. W.; Inman, B. A.; Vujaskovic, Z. Thermal dosimetry characteristics of deep regional heating of non-muscle invasive bladder cancer. *Int. J. Hyperther.* **2014**, *30*, 176−183.
(21) Liu, G.; Shen, H.; Mao, J.; Zhang, L.; Jiang, Z.; Sun, T.; Lan, Q.; Zhang, Z. Transferrin modified graphene oxide for glioma-targeted drug delivery: in vitro and in vivo evaluations. *ACS Appl. Mater. Interfaces* **2013**, *5*, 6909−6914.
(22) Cho, Y.-S.; Yoon, T.-J.; Jang, E.-S.; Soo Hong, K.; Young Lee, S.; Ran Kim, O.; Park, C.; Kim, Y.-J.; Yi, G.-C.; Chang, K. Cetuximab-conjugated magneto-fluorescent silica nanoparticles for in vivo colon cancer targeting and imaging. *Canc. Lett.* **2010**, *299*, 63−71.
(23) Lee, C.-S.; Kim, H.; Yu, J.; Yu, S. H.; Ban, S.; Oh, S.; Jeong, D.; Im, J.; Baek, M. J.; Kim, T. H. Doxorubicin-loaded oligonucleotide conjugated gold nanoparticles: A promising in vivo drug delivery system for colorectal cancer therapy. *Eur. J. Med. Chem.* **2017**, *142*, 416−423.
(24) Zeinali Sehrig, F.; Majidi, S.; Nikzamir, N.; Nikzamir, N.; Nikzamir, M.; Akbarzadeh, A. Magnetic nanoparticles as potential candidates for biomedical and biological applications. *Artif. Cells, Nanomed., Biotechnol.* **2016**, *44*, 918−927.
(25) Davis, M. E.; Chen, Z.; Shin, D. M. Nanoparticle therapeutics: an emerging treatment modality for cancer. *Nanoscience and Nanotechnology*; World Scientific Series in Nanoscience and Nanotechnology; World Scientific, 2010; pp 239−250.
(26) Oltolina, F.; Peigneux, A.; Colangelo, D.; Clemente, N.; D'Urso, A.; Valente, G.; Iglesias, G. R.; Jiménez-Lopez, C.; Prat, M. Biomimetic Magnetite Nanoparticles as Targeted Drug Nanocarriers and Mediators of Hyperthermia in an Experimental Cancer Model. *Cancers* **2020**, *12*, 2564.
(27) Hans, M. L.; Lowman, A. M. Biodegradable nanoparticles for drug delivery and targeting. *Curr. Opin. Solid State Mater. Sci.* **2002**, *6*, 319−327.
(28) Ahmad, A.; Gupta, A.; Ansari, M. M.; Vyawahare, A.; Jayamurugan, G.; Khan, R. Hyperbranched Polymer-Functionalized Magnetic Nanoparticle-Mediated Hyperthermia and Niclosamide Bimodal Therapy of Colorectal Cancer Cells. *ACS Biomater. Sci. Eng.* **2019**, *6*, 1102−1111.
(29) Alphandéry, E.; Faure, S.; Seksek, O.; Guyot, F.; Chebbi, I. Chains of magnetosomes extracted from AMB-1 magnetotactic bacteria for application in alternative magnetic field cancer therapy. *ACS Nano* **2011**, *5*, 6279−6296.
(30) Tseng, H.-Y.; Lee, G.-B.; Lee, C.-Y.; Shih, Y.-H.; Lin, X.-Z. Localised heating of tumours utilising injectable magnetic nanoparticles for hyperthermia cancer therapy. *IET Nanobiotechnol.* **2009**, *3*, 46−54.
(31) Basel, M. T.; Balivada, S.; Wang, H.; Shrestha, T. B.; Seo, G. M.; Pyle, M.; Ayabaweera, G.; Dani, R.; Koper, O. B.; Tamura, M.; Chikan, V.; Bossmann, S. H.; Troyer, D. L. Cell-delivered magnetic nanoparticles caused hyperthermia-mediated increased survival in a murine pancreatic cancer model. *Int. J. Nanomed.* **2012**, *7*, 297.
(32) Raoof, M.; Cisneros, B. T.; Corr, S. J.; Palalon, F.; Curley, S. A.; Koshkina, N. V. Tumor selective hyperthermia induced by short-wave capacitively-coupled RF electric-fields. *PloS One* **2013**, *8*, No. e68506.
(33) Minaei, S. E.; Khoei, S.; Khoee, S.; Vafashoar, F.; Mahabadi, V. P. In vitro anti-cancer efficacy of multi-functionalized magnetite nanoparticles combining alternating magnetic hyperthermia in glioblastoma cancer cells. *Mater. Sci. Eng. C* **2019**, *101*, 575−587.
(34) Li, S.; Wang, A.; Jiang, W.; Guan, Z. Pharmacokinetic characteristics and anticancer effects of 5-fluorouracil loaded nanoparticles. *BMC Cancer* **2008**, *8*, 103.
(35) Zhang, J.; Misra, R. D. K. Magnetic drug-targeting carrier encapsulated with thermosensitive smart polymer: Core−shell nanoparticle carrier and drug release response. *Acta Biomater.* **2007**, *3*, 838−850.
(36) Zaaba, N. I.; Foo, K. L.; Hashim, U.; Tan, S. J.; Liu, W.-W.; Voon, C. H. Synthesis of graphene oxide using modified hummers method: solvent influence. *Procedia Eng.* **2017**, *184*, 469−477.
(37) Liu, M.; Chen, C.; Hu, J.; Wu, X.; Wang, X. Synthesis of magnetite/graphene oxide composite and application for cobalt (II) removal. *J. Phy. Chem. C* **2011**, *115*, 25234−25240.
(38) Sapareto, S. A.; Dewey, W. C. Thermal dose determination in cancer therapy. *Int. J. Radiat. Oncol., Biol., Phys.* **1984**, *10*, 787−800.

https://doi.org/10.1021/acsomega.1c01763
ACS Omega 2021, 6, 20192−20204